nature geoscience

Article

https://doi.org/10.1038/s41561-023-01249-5

Deep formation of Earth's earliest continental crust consistent with subduction

Received: 21 December 2022

Accepted: 13 July 2023

Published online: 24 August 2023

Check for updates

Alan R. Hastie[1] ✉, Sally Law[1], Geoffrey D. Bromiley[1], J. Godfrey Fitton[1], Simon L. Harley[1] & Duncan D. Muir[2]

About four billion years ago, Earth's outer layer is thought to have been composed mostly of a 25- to 50-km-thick basaltic crust that differentiated to form the oldest stable continental crust. However, the tectonic processes responsible for the formation of this continental material remain controversial. Suggested explanations include convergent plate boundary processes akin to subduction operating today and a variety of relatively shallow (<50 km) non-plate-tectonic intracrustal mechanisms. Here we perform high-pressure–temperature melting experiments on an oceanic plateau analogue for the early basaltic crust and show that magmas with the composition of the early continental crust cannot form at pressures <1.4 GPa (~50 km depth). This suggests that Eoarchaean continental magmas are formed in deep (>50 km) subduction-like environments. Our results support previous Eoarchaean field evidence and analyses of igneous rocks that date to 4.0–3.6 billion years ago, which are consistent with subduction-like processes and suggest a primitive type of plate tectonics operated as long as 4 billion years ago on early Earth.

Plate tectonics on modern Earth creates a perpetual cycle of magmatism, erosion, deposition and mountain building that generates new continental crust. Evidence from zircons suggests that felsic material existed >4.0 billion years ago (Ga)[1], but it is only from the Eoarchaean era (4.0–3.6 Ga) that the oldest continental crust has been preserved[2,3]. Nevertheless, although we understand how plate tectonics forms continental crust on present-day Earth, there is still debate concerning the tectonic processes that formed continental crust 4.0–3.6 Ga. Volcanism associated with early Earth tectonics would have released gases to modify the early atmosphere[4], and if these gases were reducing (CO and CH_4), they could potentially provide a source for the prebiotic molecules that led to the origin of life on Earth[5]. Consequently, identification of these early Earth processes is critical to our understanding of how our planet began its evolutionary path towards our modern habitable world. Furthermore, while relatively thick basaltic crust predominates on Mars and Venus, silicic rocks (analogous to continental crust?) are also found there[6,7], albeit in much smaller volume. Determining how continental crust initially developed on Earth may help us understand the early tectonic processes operating on other rocky planetary bodies in the Solar System and beyond.

Many researchers consider that, before the formation of silicic continental crust, the crust of the Eoarchaean Earth was 25–50 km thick and dominantly mafic in composition[8–10]. The preserved continental crust from ~4.0 Ga is composed mostly of Eoarchaean tonalites and trondhjemites (ETT) that are thought to have formed by partial melting of metamorphosed basaltic (metabasic) rocks[11,12] followed by magmatic differentiation processes[13,14]. Granodiorites (G) are commonly included as a TTG suite, but they, and associated potassic granites, are generally ≤3.65 Gyr old and are interpreted as being derived from melting older ETT[15]. Therefore, to identify the mechanisms responsible for the formation of the earliest preserved continental crust, we focus on the formation of ETT-like magma. One frequently expressed view is that modern-style plate tectonic-like processes did not occur on early Earth[10,16,17] and the thick basaltic crust was not formed at mid-ocean ridges and did not sink in primitive subduction zones. However, if this is true, then the initial basaltic crust must somehow have undergone partial melting to form the oldest preserved continental material in alternative tectonic settings. Geodynamic and thermodynamic modelling suggest that partial melting of the base of the initial basaltic crust, via heating from the mantle, and/or partial melting within the crust due

[1]School of GeoSciences, University of Edinburgh, Edinburgh, UK. [2]School of Earth and Environmental Sciences, Cardiff University, Cardiff, UK.
✉e-mail: ahastie@ed.ac.uk

to intracrustal resurfacing, overturn and burial are viable options for forming the oldest continental crust[17–19].

ETT mostly have >65 wt% SiO_2, >15 wt% Al_2O_3, MgO contents from ~0.2 to 2.6 wt% and Na_2O commonly >3 wt%. They have strongly fractionated rare-earth elements (REEs) (expressed as high (La/Yb)cn, where cn indicates normalization to chondrite), high Sr/Y and low heavy (H) REE concentrations[15,20]. They also have pronounced negative Nb–Ta–Ti anomalies on normal mid-ocean-ridge basalt (N-MORB)-normalized multi-element diagrams. These ETT trace-element contents reflect (1) residual mineral phases during partial melting of the metabasic source that retain Sr in residual plagioclase, the HREEs in residual garnet and Nb–Ta–Ti in residual amphibole and/or rutile[21]; (2) compositional variability of the metabasic source region[22]; and (3) subsequent differentiation processes in ascending ETT magmas[13,14]. For (1), garnet is considered to be stable deeper than ~30 km (>1 GPa) and plagioclase at depths to ~60 km (~1.8 GPa)[23–25]. Yet in petrological experiments and thermodynamic models, garnet can be stabilized at pressures <1 GPa while plagioclase can remain at pressures of up to 2.7 GPa (refs. 17,26,27) depending on the composition of the starting material. Therefore, determining the stability ranges of residual plagioclase and garnet in >3.6-Gyr-old thick basaltic crust source rocks is paramount because these phases control the Sr and HREE contents of ETT magmas. Investigating the stability range of amphibole, which contains water, is critical as it controls dehydration melting reactions, and it may be responsible for the negative Nb–Ta–Ti anomalies in ETT rocks[21,23]. Rutile has been reported from 0.7 to 1.60 GPa (~25–55 km)[8,28,29], and determining its stability range in basaltic crustal source rocks is also essential because, like amphibole, it could explain the negative Nb–Ta–Ti anomalies in ETT.

For (2), many studies suggest that the early basaltic crust was compositionally similar to primitive basalts in Mesozoic oceanic plateau crust[23,30–33]. Metabasic source rocks for younger Archaean TTG may be more evolved than primitive oceanic plateau compositions[17,34], and upper crustal sections preserved in Eoarchaean terranes contain basalts with island-arc-like compositions[35,36]. However, in the earliest Eoarchaean, estimated ambient (non-plume) mantle potential temperatures were 1,500–1,650 °C and would produce 25–35% partial melt on decompression, generating a 25- to 50-km-thick crust composed of basalt similar in composition to primitive Mesozoic oceanic plateau basalts with Mg# > 0.6 (atomic $Mg/(Mg + Fe^{2+})$)[32]. Consequently, if the oldest preserved continents are derived from in situ intracrustal partial melting of basaltic crust, oceanic plateau-like basaltic source rocks should undergo fusion at depths <50 km to form ETT magmas in equilibrium with an amphibole-, plagioclase-, garnet- and rutile-bearing residue. In this Article, we report the results of high-pressure–temperature experiments carried out on primitive ocean-plateau basalt to test this hypothesis.

Experimentally testing an intracrustal origin for the earliest continental magmas

We investigated the partial melting of Eoarchaean basaltic crust through a series of high-pressure–temperature experiments using primitive (Mg# > 60) oceanic plateau basalts as starting materials. The samples selected represent the most primitive basaltic magma that formed the southwestern Pacific Ontong Java Plateau (OJP; samples 1187-8 and 1187-10; ref. 37). The OJP contains primitive lavas that have a high Mg# and were derived from mantle with a potential temperature of 1,500–1,600 °C (refs. 38,39). The OJP starting compositions that we use in our experiments are therefore an analogue for an early Earth basaltic crust composition. In a series of experiments, we subjected the samples to pressures and temperatures applicable to the deepest crustal levels of the Eoarchaean crustal lid—1.2–1.4 GPa (~40–50 km) assuming an early Earth crustal geothermal gradient of 20–30 °C km^{-1} (refs. 10,16); a higher gradient would result in melting at shallower levels. Pressures of 1.2–1.4 GPa were chosen because they are the highest pressures prevailing in a basaltic intracrustal environment and are more likely to stabilize residual garnet and rutile. Failure to stabilize garnet and rutile at 1.2–1.4 GPa would imply that ETT magmas could not have been generated from metamorphosed oceanic plateau-like material in situ within the early Archaean mafic crust.

Water is required to stabilize residual amphibole, but in the absence of subduction it may be difficult to transport water to great depths. However, the basaltic crust may not have been stagnant, and geodynamic modelling suggests that processes such as crustal resurfacing and overturn[17–19] could have buried water into the lower crust in the Eoarchaean. Recently[33], $Fe^{3+}/\Sigma Fe$ values from Archaean volcanic rocks in Pilbara were used to suggest a water content of 1.9 wt% for TTG source rocks. From 1.2 to 1.4 GPa, dehydration melting due to amphibole breakdown should occur at ≥900 °C (refs. 40,41) at the geothermal gradients expected in the Eoarchaean[16]. Although unlikely, it could also be argued that ETT magmas are derived from underplated relatively anhydrous basic rocks that form part of the base of the basaltic crust[42]. To test the two endmember scenarios, we ran anhydrous and hydrous (~2 wt% water) experiments at 1.2–1.4 GPa. The hydrous experiments were designed to maximize the likelihood of stabilizing residual amphibole in the simulated lower crust by assuming a relatively low early Earth geothermal gradient (~20–25 °C km^{-1}). Through this strategy, we sought to maximize the likelihood of stabilizing residual garnet, rutile and amphibole and generating ETT-like melts.

All the anhydrous experiments produced partial melt in equilibrium with clinopyroxene, orthopyroxene and plagioclase-bearing residues. The experimental partial melts have the composition of tholeiitic basalts with 49.53–52.46 wt% SiO_2, 1.01–2.15 wt% TiO_2, 9.53–13.20 wt% FeO, 4.00–7.21 wt% MgO and $Na_2O + K_2O$ contents of 2.06–2.96 wt%. These partial melts do not have the major-element composition of ETT, and their mafic compositions are predictable from simple phase petrology in the forsterite–silica system, which prohibits the formation of silicic partial melts from anhydrous olivine–normative compositions by partial melting or fractional crystallization at depths >0.5 GPa. The lack of residual amphibole, garnet and rutile have a strong influence on the trace-element composition of the anhydrous partial melts. Unlike ETT, the anhydrous partial melts have flat N-MORB-normalized patterns, relatively high HREE concentrations, no negative Nb or Ti anomalies and relatively low large-ion lithophile element (LILE; Ba, K, Sr) and light (L) REE abundances (La–Nd) (Fig. 1a). By contrast, the hydrous experiments generate tonalitic partial melts (Fig. 1b) with 60.17–72.70 wt% SiO_2, 0.14–0.51 wt% TiO_2, 14.60–21.07 wt% Al_2O_3, 1.67–3.98 wt% FeO, 1.17–3.43 wt% MgO, high Na_2O up to 5.24 wt% and relatively low K_2O of 0.21–1.10 wt% (average $K_2O/Na_2O < 0.6$). The hydrous melts are in equilibrium with residues of amphibole, clinopyroxene, orthopyroxene, plagioclase and titanomagnetite, and as with the anhydrous experiments, garnet and rutile are absent. Residual amphibole and titanomagnetite result in partial melts with lower FeO contents and negative Ti anomalies as seen in ETT (Fig. 1a). However, once more, the residual mineralogy imparts N-MORB-normalized trace-element patterns on the resultant melts that differ from ETT, particularly the absence of negative Nb anomalies (Fig. 1a).

On a Sr/Y–Y plot (Fig. 1c), all experimental anhydrous and hydrous partial melts plot away from ETT. The lack of negative Nb anomalies is seen on the La/Nb_{mn} (N-MORB-normalized)–Gd/Ti_{mn} diagram (Fig. 1d), and the flat REE patterns of the hydrous melts, which strongly contrast with published ETT, are highlighted in the La/Nb_{mn}–Gd/Yb_{mn} plot (Fig. 1e). It is likely that ETT magma compositions were modified by fractional crystallization processes during ascent[13,14]. We model fractional crystallization trends on our experimental partial melts by calculating amphibole, clinopyroxene and plagioclase crystallization vectors for average anhydrous and hydrous melts in Fig. 1c–e. In the Sr/Y–Y diagram, amphibole crystallization can drive our experimental partial melts to ETT-like compositions (Fig. 1c), but the same amphibole crystallization drives our partial melt compositions farther away from ETT

https://doi.org/10.1038/s41561-023-01249-5

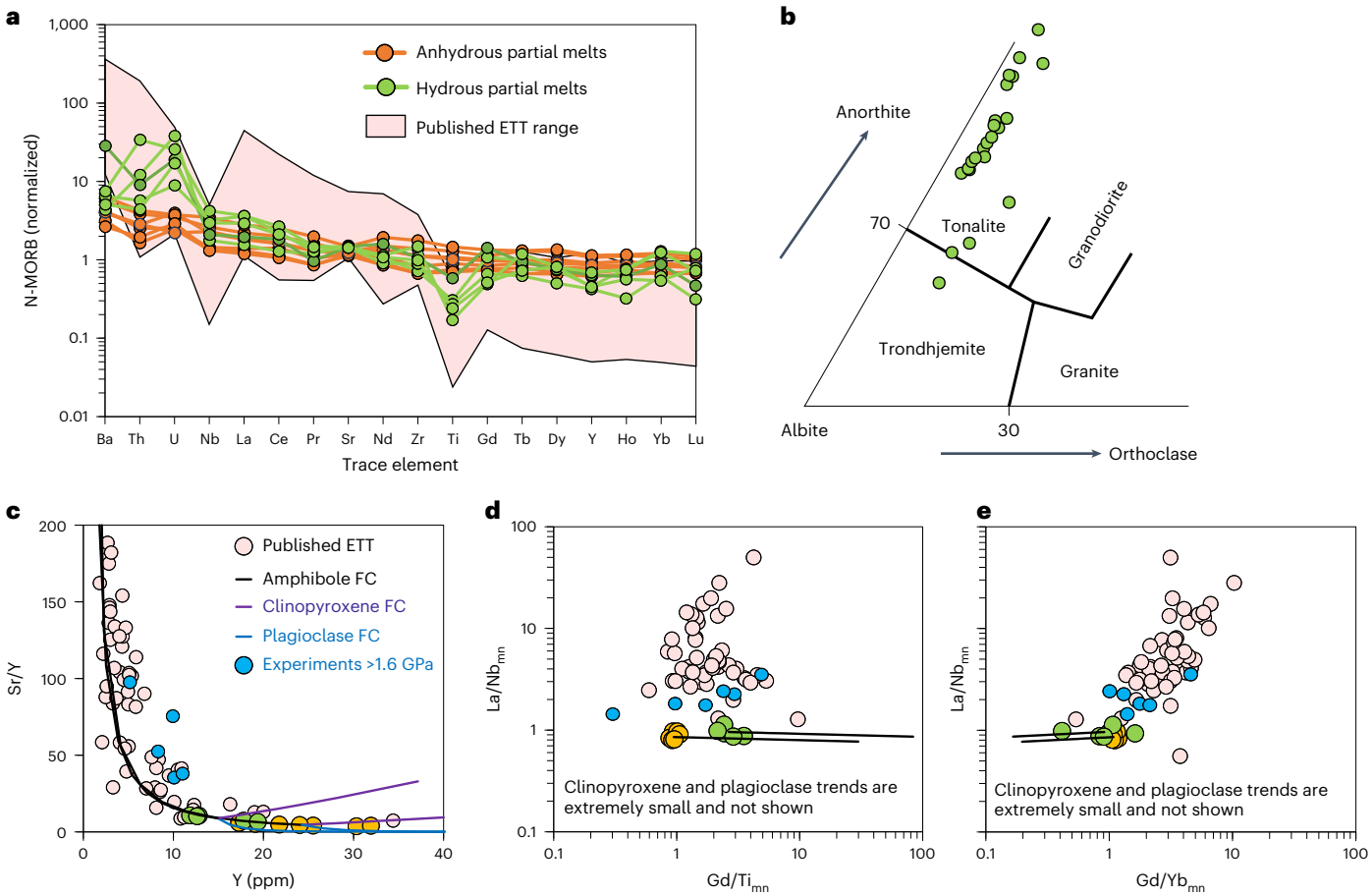

Fig. 1 | Major- and trace-element partial melt data from our experiments. a, N-MORB-normalized plot showing ETT[15,20,48–50] and trace-element results from our experiments. **b**, Anorthite–albite–orthoclase ternary diagram classifying our hydrous partial melts as tonalitic[51]. **c**–**e**, Sr/Y–Y (**c**), La/Nb_{mn}–Gd/Ti_{mn} (**d**) and La/Nb_{mn}–Gd/Yb_{mn} (**e**) diagrams. Fractional crystallization (FC) trends in **c**–**e** are calculated using the equation from ref. 52 and distribution coefficients in ref. 53. Some diagrams do not show plagioclase and clinopyroxene FC vectors because the trends are very short. Experimental data >1.6 GPa are partial melts in equilibrium with residual garnets that are generated at pressures higher than those possible in intracrustal environments[22,23].

concentrations in the La/Nb_{mn}–Gd/Ti_{mn} and La/Nb_{mn}–Gd/Yb_{mn} diagrams (Fig. 1d,e). Furthermore, clinopyroxene and plagioclase crystallization cannot generate ETT-like compositions from our experimental partial melts in any of the diagrams (Fig. 1c–e).

Significance for initial Eoarchaean continental formation

We show that ETT-like magmas cannot be generated by partial melting of anhydrous or hydrous primitive oceanic plateau-like metabasic rocks at the base of the early Eoarchaean mafic crust because garnet and rutile are not stabilized at less than ~45–50 km depth (≤1.4 GPa). Garnet was stabilized in previous hydrous experiments using similar primitive metabasic starting material at higher pressures (≥1.6 GPa: >50 km)[23] (Fig. 2a). However, garnet stability is closely linked to the Mg# of the starting composition, and in general, the higher the ratio the deeper the garnet stability field. Assuming that all Fe is presented as FeO, the Mg#s of our starting compositions are 0.64–0.65, which is relatively high compared with other experimental[24,43] and thermodynamic studies[8,17]. Furthermore, the OJP experimental material has $Fe^{3+}/\Sigma Fe$ of ~0.2, which will further increase the Mg# in our starting compositions. Clinopyroxene in our residues has relatively high Al_2O_3 (7.3–10.8 wt%), which also restricts garnet growth to higher pressures. Consequently, garnet stability in our experiments is expected to be at higher pressures than was found in previous studies as our starting composition is more comparable to the primitive Eoarchaean mafic crust.

The instability of garnet at 1.4 GPa was confirmed by running a 'reverse' experiment. Previous experiments using OJP starting compositions at 2.0 GPa and 900–950 °C grew large modal volumes of garnet. An example of such an experiment (OJPgw10) is shown in Fig. 2b. In our experiments, we replicated a 2.0 GPa experiment with sample OJP4gw4, composed of glass made by fusing 1187-10. The glass was run for 24 h at 2.0 GPa, 950 °C with 2.2 wt% water added. After 24 h, the experiment was quenched, the capsule was recovered and the same capsule was run again for 48 h at 1.4 GPa and 1,000 °C. The results of OJP4gw4 after quenching the second experiment are shown in Fig. 2c. It can be clearly seen that the large garnets that grew at 2.0 GPa are unstable at 1.4 GPa and have broken down into an assemblage of plagioclase, orthopyroxene and titanomagnetite. This provides conclusive evidence that garnet is not stabilized until ~1.6 GPa (>50–55 km).

This lack of residual garnet in our experiments shows that conversion of mafic crust to eclogite or formation of garnet-rich restites during partial melting is unlikely to occur in the lower parts of the early Eoarchaean crust at pressures ≤1.4 GPa. Multiple partial melting events involving tonalites and pyroxenite residues, like those generated in this study, would also not generate ETT-like magmas. Partial melting of tonalitic material generates granodiorites and potassic granites[15], and the pyroxenite residues have an even more primitive mafic composition to further inhibit shallow garnet growth (mass-balance calculations indicate up to 13.4 wt% MgO).

https://doi.org/10.1038/s41561-023-01249-5

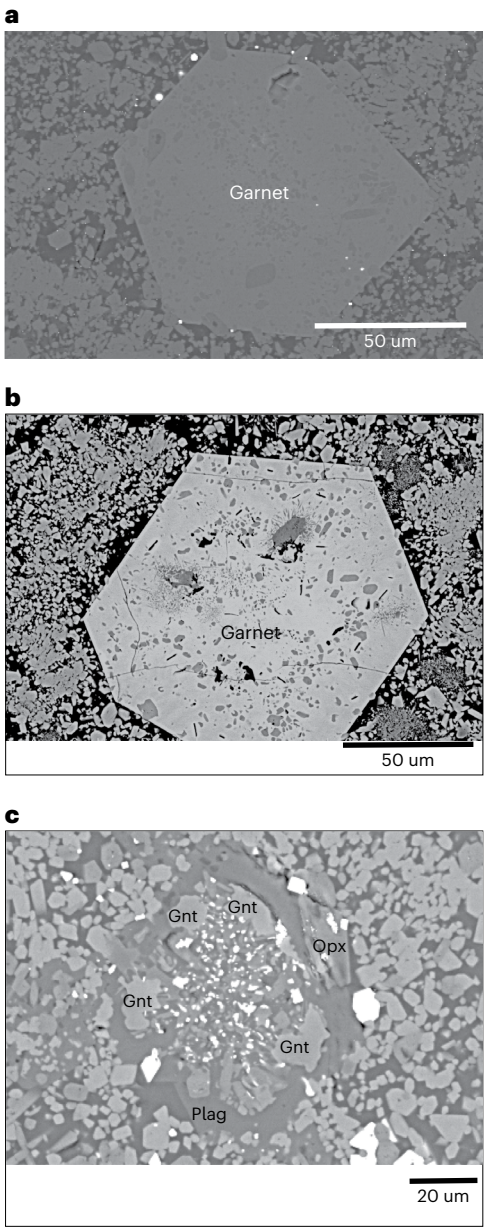

Fig. 2 | Nucleation and growth of garnet from 1.4 to 2.0 GPa. a, Representative scanning electron microscope (SEM) image of sample OJPgw18 that used 1187-8 starting material with 2.0 wt% water and was run for 24 h at 975 °C and 1.6 GPa (see Supplementary Table 2 for run conditions). **b**, SEM image of a large garnet crystal in OJPgw10 that was run at 2.0 GPa and 925 °C. **c**, Sample OJP4gw4, unstable garnet (gnt) that has broken down into plagioclase (plag), orthopyroxene (opx) and titanomagnetite after being run first for 24 h at 2.0 GPa and 950 °C and then for 48 h at 1.4 GPa and 1,000 °C.

Many published models propose garnet growth at ≥30 km to allow relatively shallow eclogitization (to garnet-rich amphibolite or garnet–clinopyroxenite) of the lower Eoarchaean mafic crust to trigger delamination and foundering of mafic crust into the mantle[9,19,24,44]. However, our experiments invalidate geodynamic models for the Eoarchaean Earth involving continent-forming mechanisms that are driven by eclogitization of the lower crust using primitive oceanic plateau-like compositions.

Surviving fragments of Eoarchaean crust also include diverse meta-volcanic rocks with Eoarchaean island-arc-like basalt (EIAB) compositions (for example, negative Nb anomalies on multi-element diagrams)[15,35,36]. Field studies on Eoarchaean terranes[36] and previous geochemical investigations[20] suggest that ETT could be, at least in part, derived from the partial melting of EIAB. Importantly, it has been proposed that EIAB, and thus the possible ultimate source for Earth's oldest preserved continents, may be derived from the partial melting of a metabasic crustal precursor[17] that would be represented by our oceanic plateau-like starting composition. Nevertheless, our experiments rule out the formation of EIAB by fusing metabasic rocks at ~40–50 km because rutile cannot be stabilized under these conditions to generate the negative Nb–Ta anomalies in EIAB.

The formation of ETT, and the oldest preserved continental crust, requires deeper tectonic environments than the shallow, in situ intracrustal settings frequently proposed. If ETT magmas were derived from primitive oceanic plateau-like metabasic rocks, source regions deeper than ~50 km and relatively low geothermal gradients are required to convert primitive basalt to metabasic rocks that can undergo partial melting in equilibrium with an amphibole-, garnet- and rutile-bearing residue. Of all the processes that have been proposed for the formation of ETT, only crustal drips (dripduction) and subduction satisfy these criteria. However, the absence of garnet in the lower crust would make it much more difficult to initiate the gravitational instability required to drive crustal drips and delamination, so that subduction is the only viable mechanism for forming the earliest continental crust. If ETT were derived from a metabasic source with EIAB compositions, this cannot have been generated from a primitive Eoarchaean mafic crustal precursor. Thus, EIAB may require partial melting of a mantle source to which a fluid/melt component has been added from a deeper source region with residual rutile[35]. In the absence of large volumes of mature continental crust in the Eoarchaean, the most plausible mechanism to form EIAB is also by primitive subduction-like processes[20,35].

Eoarchaean tectonic imbrication (especially in the Isua supracrustal belt and adjacent areas in Greenland[45]) and the seismic and electrical anomalies detected below the Archaean Slave Craton, Canada, are both thought to be vestigial reflections of convergence above ancient subduction zones[15,35,36,46]. Geochemical mass-balance modelling[22] suggests that high LILE and LREE contents in ETT are best explained by mixing metabasic-derived ETT-like melts with slab-derived fluids. Olivine crystals in possible Eoarchaean mantle rocks show B-type lattice orientation that is seen only in mantle wedge-derived rocks[47], and growing evidence for ultra-high-pressure metamorphism in Eoarchaean meta-peridotites suggests subduction-like processes[45]. Using our experimental results alongside such other evidence, we propose that primitive plate tectonic processes in the Eoarchaean led to the generation of ETT, and thus the oldest preserved continental crust, in proto-subduction zones. As the continents stabilized and then began to grow, accompanying volcanism released gases into the primitive atmosphere, and weathering and erosion of the early landmasses deposited sedimentary material into Earth's oceans to be recycled into the mantle or to form new continental crust. Thus, Eoarchaean plate tectonics and continental growth were responsible for modifying early Earth's interior and crustal surface and are pivotal to our understanding of how Earth evolved into our modern world.

Online content

Any methods, additional references, Nature Portfolio reporting summaries, source data, extended data, supplementary information, acknowledgements, peer review information; details of author contributions and competing interests; and statements of data and code availability are available at https://doi.org/10.1038/s41561-023-01249-5.

References

1. O'Neil, J. et al. in *Earth's Oldest Rocks* (eds Van Kranendonk, M. J. et al.) 219–250 (Elsevier, 2007).

2. Bowring, S. A. & Williams, I. S. Priscoan (4.00-4.03 Ga) orthogneisses from northwestern Canada. *Contrib. Mineral. Petrol.* **134**, 3–16 (1999).
3. Nutman, A. P., Bennett, V. C., Friend, C. R. L., Horie, K. & Hidaka, H. ~3,850 Ma tonalites in the Nuuk region, Greenland: geochemistry and their reworking within an Eoarchaean gneiss complex. *Contrib. Mineral. Petrol.* **154**, 385–408 (2007).
4. Kharecha, P., Kasting, J. & Siefert, J. A coupled atmosphere–ecosystem model of the early Archean Earth. *Geobiology* **3**, 53–76 (2005).
5. Sleep, N. H., Bird, D. K. & Pope, E. C. Serpentinite and the dawn of life. *Phil. Trans. R. Soc. B* **366**, 2857–2869 (2011).
6. Sautter, V. et al. In situ evidence for continental crust on early Mars. *Nat. Geosci.* **8**, 605–609 (2015).
7. Shellnutt, J. G. Derivation of intermediate to silicic magma from the basalt analyzed at the Vega 2 landing site, Venus. *PLoS ONE* **13**, e0194155 (2018).
8. Palin, R. M., White, R. W. & Green, E. Partial melting of metabasic rocks and the generation of tonalitic–trondhjemitic–granodioritic (TTG) crust in the Archaean: constraints from phase equilibrium modelling. *Precambrian Res.* **287**, 73–90 (2016).
9. Hawkesworth, C. J., Cawood, P. A., Dhuime, B. & Kemp, T. I. S. Earth's continental lithosphere through time. *Annu. Rev. Earth Planet. Sci. Lett.* **45**, 169–198 (2017).
10. Smithies, R. H. et al. Oxygen isotopes trace the origins of Earth's earliest continental crust. *Nature* **592**, 70–75 (2021).
11. Rapp, R. P., Shimizu, N. & Norman, M. D. Growth of early continental crust by partial melting of eclogite. *Nature* **425**, 605–608 (2003).
12. Foley, S. F., Tiepolo, M. & Vannucci, R. Growth of early continental crust controlled by melting of amphibolite in subduction zones. *Nature* **417**, 837–840 (2002).
13. Rollinson, H. Do all Archaean TTG rock compositions represent former melts? *Precambrian Res.* **367**, 106448 (2021).
14. Kendrick, J., Duguet, M. & Yakymchuk, C. Diversification of Archean tonalite–trondhjemite–granodiorite suites in a mushy middle crust. *Geology* **50**, 76–80 (2022).
15. Nutman, A. P. et al. in *Earth Accretionary Systems in Space and Time* (eds Cawood, P. A. & Kröner, A.) 127–154 (Geological Society of London, 2009).
16. Brown, M. & Johnson, T. Time's arrow, time's cycle: granulite metamorphism and geodynamics. *Mineral. Mag.* **83**, 323–338 (2019).
17. Johnson, T. E., Brown, M., Gardiner, N. J., Kirkland, C. L. & Smithies, H. Earth's first stable continents did not form by subduction. *Nature* **543**, 239–242 (2017).
18. Rozel, A. B., Golabek, G. J., Jain, C., Tackley, P. J. & Gerya, T. Continental crust formation on early Earth controlled by intrusive magmatism. *Nature* **545**, 332–335 (2017).
19. Sizova, E., Gerya, T., Stuwe, K. & Brown, M. Generation of felsic crust in the Archean: a geodynamic modeling perspective. *Precambrian Res.* **271**, 198–224 (2015).
20. Hoffmann, J. E. et al. Mechanisms of Archean crust formation inferred from high-precision HFSE systematics in TTGs. *Geochim. Cosmochim. Acta* **75**, 4157–4178 (2011).
21. Martin, H., Smithies, R. H., Rapp, R., Moyen, J.-F. & Champion, D. An overview of adakite, tonalite–trondhjemite–granodiorite (TTG), and sanukitoid: relationships and some implications for crustal evolution. *Lithos* **79**, 1–24 (2005).
22. Hastie, A. R. & Fitton, J. G. Eoarchaean tectonics: new constraints from high pressure–temperature experiments and mass balance modelling. *Precambrian Res.* **325**, 20–38 (2019).
23. Hastie, A. R., Fitton, J. G., Bromiley, G. D., Butler, I. B. & Odling, N. W. A. The origin of Earth's first continents and the onset of plate tectonics. *Geology* **44**, 855–858 (2016).
24. Zhang, C. et al. Contraints from experimental melting of amphibolite on the depth of formation of garnet-rich restites, and implications for models of early Archean crustal growth. *Precambrian Res.* **231**, 206–217 (2013).
25. Sen, C. & Dunn, T. Dehydration melting of a basaltic composition amphibolite at 1.5 and 2.0 GPa: implications for the origin of adakites. *Contrib. Mineral. Petrol.* **117**, 394–409 (1994).
26. Johnson, T. E. et al. An impact melt origin for Earth's oldest known evolved rocks. *Nat. Geosci.* **11**, 795–799 (2018).
27. Rapp, R. P. & Watson, E. B. Dehydration melting of metabasalt at 8–32 kbar: implications for continental growth and crust–mantle recycling. *J. Petrol.* **36**, 891–931 (1995).
28. Xiong, X. L., Adam, J. & Green, T. H. Rutile stability and rutile/melt HFSE partitioning during partial melting of hydrous basalt: implications for TTG genesis. *Chem. Geol.* **218**, 339–359 (2005).
29. Patiño Douce, A. E. & Beard, J. S. Dehydration-melting of biotite gneiss and quartz amphibolite from 3 to 15 kbar. *J. Petrol.* **36**, 707–738 (1995).
30. Kerrich, R. & Polat, A. Archean greenstone–tonalite duality: thermochemical mantle convection models or plate tectonics in the early Earth global dynamics? *Tectonophysics* **415**, 141–165 (2006).
31. Smithies, R. H., Champion, D. C. & Cassidy, K. F. Formation of Earth's early Archaean continental crust. *Precambrian Res.* **127**, 89–101 (2003).
32. Tarney, J. & Jones, C. E. Trace element geochemistry of orogenic igneous rocks and crustal growth models. *J. Geol. Soc. Lond.* **151**, 855–868 (1994).
33. Hawkesworth, C. J. & Kemp, A. I. S. A Pilbara perspective on the generation of Archaean continental crust. *Chem. Geol.* **578**, 120326 (2021).
34. Smithies, R. H., Champion, D. C. & Van Kranendonk, M. J. Formation of Paleoarchean continental crust through infracrustal melting of enriched basalt. *Earth Planet. Sci. Lett.* **281**, 298–306 (2009).
35. Jenner, F. E. et al. Evidence for subduction at 3.8 Ga: geochemistry of arc-like metabasalts from the southern edge of the Isua Supracrustal Belt. *Chem. Geol.* **261**, 83–98 (2009).
36. Polat, A. & Hoffmann, A. W. Alteration and geochemical patterns in the 3.7–3.8 Ga Isua greenstone belt, West Greenland. *Precambrian Res.* **126**, 197–218 (2003).
37. Fitton, J. G. & Godard, M. in *Origin and Evolution of the OJP* (eds Fitton, J. G. et al.) 151–178 (Geological Society of London, 2004).
38. Herzberg, C. & Asimow, P. D. PRIMELT3 MEGA.XLSM software for primary magma calculation: peridotite primary magma MgO contents from the liquidus to the solidus. *Geochem. Geophys. Geosyst.* **16**, 563–578 (2015).
39. Hastie, A. R. et al. The composition of mantle plumes and the deep Earth. *Earth Planet. Sci. Lett.* **444**, 13–25 (2016).
40. Peacock, S. M., Rushmer, T. & Thompson, A. B. Partial melting of subducting oceanic crust. *Earth Planet. Sci. Lett.* **121**, 227–244 (1994).
41. Moyen, J.-F. & Stevens, G. in *Archean Geodynamics and Environments* Vol. 164 (eds Benn, K. et al.) 149–175 (AGU, 2006).
42. Harley, S. L. The origin of granulites: a metamorphic perspective. *Geol. Mag.* **126**, 215–247 (1989).
43. Winther, K. T. An experimentally based model for the origin of tonalitic and trondhjemitic melts. *Chem. Geol.* **127**, 43–59 (1996).
44. Wiemer, D., Schrank, C. E., Murphy, D. T., Wenham, L. & Allen, C. M. Earth's oldest stable crust in the Pilbara Craton formed by cyclic gravitatinal overturns. *Nat. Geosci.* **11**, 357–361 (2018).
45. Nutman, A. P., Friend, C. R. L., Bennett, V. C., Keewook, Y. & Van Kranendonk, M. Review of the Isua supracrustal belt area (Greenland) Eoarchean geology from integrated 1:20,000 scale

maps, field observations and laboratiry data: constraints on early geodynamics. *Precambrian Res.* **379**, 106785 (2022).
46. Chen, C.-W., Rondenay, S., Evans, R. L. & Snyder, D. B. Geophysical detection of relict metasomatism from an Archaen (~3.5 Ga) subduction zone. *Science* **326**, 1089–1091 (2009).
47. Kaczmarek, M.-A., Reddy, S. M., Nutman, A. P., Friend, C. R. L. & Bennett, V. C. Earth's oldest mantle fabrics indicate Eoarchaean subduction. *Nat. Commun.* **7**, 10665 (2016).
48. Hoffmann, J. E., Nagel, T. J., Munker, C., Naeraa, T. & Rosing, M. T. Constraining the process of Eoarchean TTG formation in the Itsaq Gneiss Complex, southern West Greenland. *Earth Planet. Sci. Lett.* **388**, 374–386 (2014).
49. Kamber, B. S., Ewart, A., Collerson, K. D., Bruce, M. C. & McDonald, G. D. Fluid-mobile trace element constraints on the role of slab melting and implications for Archaean crustal growth models. *Contrib. Mineral. Petrol.* **144**, 38–56 (2002).
50. Ge, R., Zhu, W., Wilde, S. A. & Wu, H. Remnants of Eoarchean continental crust derived from a subducted proto-arc. *Sci. Adv.* **4**, eaao3159 (2018).
51. Barker, F. in *Trondhjemites, Dacites and Related Rocks* (ed Barker, F.) 1–12 (Elsevier, 1979).
52. Shaw, D. M. Trace element fractionation during anatexis. *Geochim. Cosmochim. Acta* **34**, 237–243 (1970).
53. Bédard, J. H. A catalytic delamination-driven model for coupled genesis of Archaean crust and sub-continental lithospheric mantle. *Geochim. Cosmochim. Acta* **70**, 1188–1214 (2006).

Methods

High-pressure–temperature experiments

Experimental runs were carried out on a half-inch (1.27 cm) end-loaded piston cylinder press at the NERC Recognised Experimental Geoscience Laboratories, School of GeoSciences, University of Edinburgh, using talc–Pyrex–graphite assemblies. Capsules were centred in assemblies using alumina spacers, within 1 mm of the thermocouple junction. Experiments were carried out using the hot-piston-out technique in which runs were pressurized to 110% of the reported final pressure, heated and pressure allowed to bleed off to the desired run pressure. Pressure was monitored and maintained during runs within 0.25 kbar of the reported pressure. A 15%, correction to nominal pressure was applied to compensate for pressure loss due to internal friction, previously calibrated for the assembly on the basis of the quartz–coesite transition, the kyanite–sillimanite transition, the jadeite–albite–quartz reaction and the melting point of diopside. Temperature was measured with a Pt-Pt13%Rh thermocouple. No correction for the effect of pressure on thermocouple electromotive force was applied. Temperature gradients across the sample are small over the temperature range used here, on the order of 10 °C, and temperature during runs did not deviate more than 5 °C from the reported values. Experiments were quenched by shutting off power to the heating circuit, which led to the temperature falling to below 300 °C after 3–5 s, and to below 100 °C after 8–10 s.

The first sample used as starting material consisted of a finely powdered natural glass sample (primitive, depleted and anhydrous Kroenke-basalt sample: 1187-8; ref. 37), with up to ~3 vol.% of crystallized olivine, from the OJP. However, there was not enough 1187-8 material to complete the twelve experiments, so a very similar OJP powdered rock sample, 1187-10; ref. 37, was glassed in an atmosphere-controlled Deltech vertical tube gas-mixing furnace for subsequent experiments. It is preferable to use glass starting compositions in experimental studies to attain a final equilibrium melt and mineral assemblage. Previous methods of using rock powders as starting compositions can result in disequilibrium end products if basalt is first converted into a metabasic protolith because the original mineralogy of the basalt does not completely break down due to slow reaction kinetics (this is shown in our reversal experiment where the garnet has not completely broken down). Thus, glass starting materials are essential in demonstrating that chemical equilibrium is attained in experiments because we 'grow' the metabasic assemblage from the glass. Phase assemblages formed under chemical equilibrium must, by definition, be independent of the mineralogical make-up of starting materials. Any difference in run products between studies using different starting materials suggest that studies reliant on use of un-equilibrated rock powders must be treated with extreme caution. In addition, use of un-equilibrated rock powders can result in chemical segregation. The entire sample cannot be considered as a single system. Instead, pre-existing mineralogy results in varying compositions over regions of the sample. The glass starting material in this study gives equilibrium melt and mineral residues (Extended Data Fig. 1).

To make the 1187-10 glass, a Pt crucible was pre-contaminated with 1187-10 material at 1,300 °C to saturate the crucible with Fe. The initial 1187-10 material was removed from the crucible and ~2 g of new powder was added. This new powder was fused in the furnace at 1,300 °C for 25 min in a stream of CO_2–H_2 gas. In-line Bronkhorst Ltd mass-flow controllers were used to accurately control and monitor gas flow. Deines (1970) tables were used to determine gas proportions required to anneal the sample at an oxygen fugacity close to that of the Ni–NiO (NNO) buffer, calibrated at run conditions using a zirconium dioxide oxygen sensor. The procedure aimed to limit the time available for Fe loss to the capsule and volatile element (for example, K) loss to the furnace atmosphere. The synthesized 1187-10 glass was removed from the crucible and was crushed and finely powdered. Glass powder was imaged on a scanning electron microscope to ensure that the powder had fully glassed. Glass fragments were analysed (25 spot analyses) for major elements on a Cameca SX100 electron microprobe at the University of Edinburgh. Synthetic 1187-10 glass major-element compositions are near identical to the natural glass 1187-8 and the original 1187-10 powder, and we had no Fe or volatile loss (Extended Data Table 1).

Synthetic 1187-10 glass trace-element compositions were analysed in the Brian Price ICP-MS laboratory at the University of Edinburgh on a Nu Attom quadrupole inductively coupled plasma mass spectrometer (ICP-MS). The trace-element analyses were checked by also analysing synthetic glass fragments at the Scottish Universities Environmental Research Centre on an Agilent 7500ce ICP-MS. Like the major-element analyses, 1187-10 glass trace-element concentrations are near identical to the natural glass 1187-8 and the original 1187-10 powder (Extended Data Fig. 2).

Approximately 0.035–0.05 g starting material and ~2 wt% 18 MΩm deionized water for the hydrous experiments were loaded in welded $Ag_{70}Pd_{30}$ or $Au_{75}Pd_{25}$ capsules and run for 24 h. These metal alloys prevent appreciable Fe loss from the starting composition to the capsules. This was confirmed by analysing the capsule walls after experimentation and finding no Fe contamination in the metal alloy. The experiments were designed to simulate partial melting of basaltic crustal material in a dry to wet lower crustal environment, thus requiring oxygen fugacities (fO_2) close to nickel–nickel oxide (NNO) or quartz–fayalite–magnetite (QFM) mineralogical equilibrium. QFM is a complex reaction, and it is difficult to obtain true equilibrium, whereas NNO is a much simpler reaction and is only ~ΔQFM + 0.7. However, experiments cannot be buffered using an NNO assemblage due to Ni reaction with the Pd-bearing capsule material. Nevertheless, although not explicitly buffered, the talc–Pyrex experimental assembly used in this study imparts conditions within the sample volume close to the NNO oxygen buffer, consistent with Fe X-ray absorption near-edge structure spectroscopy measurements of silicate glass in other quenched run products[54]. Furthermore, the synthetic glass starting materials were pre-annealed at fO_2 close to the NNO buffer, and only minimal changes in fO_2 are expected during our partial melting experiments. Many previous fluid-absent experiments reported in the literature do not approach equilibrium, but the use of our natural and synthetic glasses enables us to do so. Equilibrium conditions in our experiments are shown by (1) all mineral phases being homogeneous and un-zoned (Extended Data Fig. 1) and (2) similar phase proportions and compositions being derived from previous experiments run for 24 and 48 h at the same pressures and temperatures[23]. A diagram showing the pressure–temperature locations of our 12 experiments is shown in Extended Data Fig. 3.

Major-element analyses

Experimental charges were encased in epoxy resin, ground down and polished for imaging and major- and trace-element analysis. Samples were carbon coated and imaged on an FEI XL30 field-emission gun environmental scanning electron microscope at the School of Earth and Environmental Sciences at Cardiff University, UK, and on a Carl Zeiss SIGMA HD VP field-emission scanning electron microscope in the School of GeoSciences at the University of Edinburgh. Elemental maps were also made at Cardiff to aid mass-balance determinations. Major-element and high-concentration trace-element analyses of run products were determined at the University of Edinburgh using a five-spectrometer Cameca SX100 electron microprobe instrument with 15 kV acceleration voltage. Mineral products were measured using a fully focused beam and two conditions of 4 nA (major elements) and 100 nA (minor and trace elements). For glass analyses, a defocused beam of 2 nA and 5 µm was used for major elements to avoid Na loss and to target the relatively small melt pools, and 80 nA at 5 µm was used for minor and trace elements.

Trace-element analyses

Trace-element analyses on the glasses were determined on a secondary ion mass spectrometer at the University of Edinburgh. Anhydrous

analyses were performed on a Cameca IMS-4f ion microprobe. Analyses were made using a 16 O^- primary beam of 10.5 keV impact energy. A 1.5 nA beam was focused to a 5–8 µm spot, and nominal 4.5 keV positive secondary ions were measured using a 75 V offset ±20 eV. Corrections were made for overlap of the LREEs on the HREEs and HoO on Ta. Concentrations were determined using a combination of GSD-1G, BCR2g, ML3b and SRM610 glass standards. Hydrous analyses were performed on a Cameca 7f-Geo ion microprobe. Analyses were made using a 16 O^- primary beam of 13 keV impact energy. A 1 nA beam was focused to a 5–8 micron spot, and nominal 5 keV positive secondary ions were measured using a 75 V offset ±20 eV. Corrections were made for overlap of the LREEs on the HREEs and HoO on Ta. Concentrations were determined using a combination of GSD-1G, BCR2g and ML3b glass standards.

Fractional crystallization modelling

The equation used for our trace-element fractional crystallization models is:

$$C_l = C_0 F^{(D-1)}$$

With C_l being the trace-element concentration in the liquid, C_0 is the initial concentration before fractional crystallization, D is the partition coefficient of the fractionating mineral in question and F is the proportion of melt remaining[52]. The C_0 values represent average anhydrous and hydrous experimental melt compositions, and the partition coefficients are from ref. 53.

Data availability

All data available in Supplementary Tables 1–4 and in the publicly accessible Figshare portal at https://figshare.com/s/e57bdbd1f09f7f5356ee.

References

54. Stokes, T. N., Bromiley, G. D., Potts, N. J., Saunders, K. E. & Miles, A. J., EIMF. The effect of melt composition and oxygen fugacity on manganese partitioning between apatite and silicate melt. *Chem. Geol.* **506**, 162–174 (2019).

Acknowledgements

The staff at the Edinburgh Materials and Micro-Analysis Centre (EMMAC), Geochemistry laboratory, Scanning Electron Microscope (SEM) facility and the Electron Probe Microanalysis (EPMA) facility are thanked for help with sample preparation and data analysis and imaging. The experimental work was funded through Leverhulme Research Grant (RPG-2019-282) and the NERC micro-analytical facility grant (IMFSC117) awarded to A.R.H.

Author contributions

A.R.H. developed the initial idea, ran half of the experiments, imaged most of the experiments on an SEM, did the EPMA and SIMS analyses and wrote most of the paper. S.L. ran several experiments, imaged the runs on an SEM and contributed to the text. G.D.B. ran two experiments and glassed the starting compositions. J.G.F. supplied the starting rocks and wrote part of the text. S.L.H. checked our metamorphic results and wrote part of the text, and D.D.M. imaged the samples and calculated modal abundances using an analytical SEM at Cardiff.

Competing interests

The authors declare no competing interests.

Additional information

Extended data is available for this paper at https://doi.org/10.1038/s41561-023-01249-5.

Supplementary information The online version contains supplementary material available at https://doi.org/10.1038/s41561-023-01249-5.

Correspondence and requests for materials should be addressed to Alan R. Hastie.

Peer review information *Nature Geoscience* thanks Allen Nutman, Chao Zhang and the other, anonymous, reviewer(s) for their contribution to the peer review of this work. Primary Handling Editors: Alison Hunt, Stefan Lachowycz and Rebecca Neely, in collaboration with the *Nature Geoscience* team.

https://doi.org/10.1038/s41561-023-01249-5

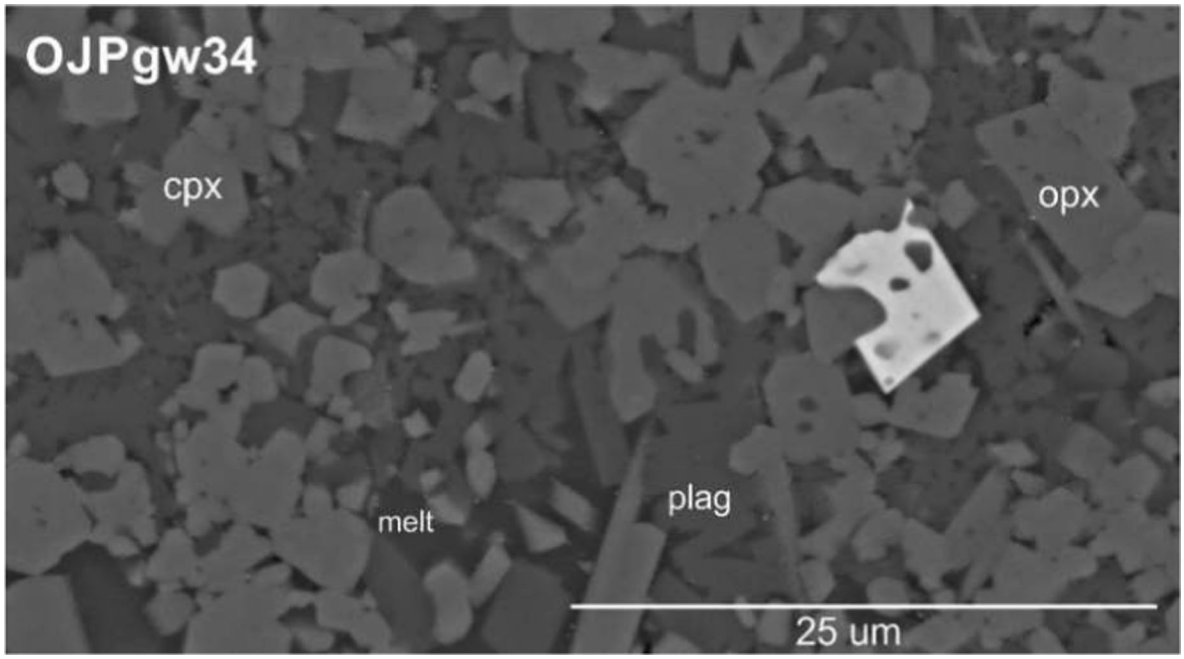

Extended Data Fig. 1 | Lack of garnet growth at 1.4 GPa. Representative scanning electron microscope image of sample OJPgw34 that was run at 950 °C and 1.2 GPa with 1.9 wt.% added water.

https://doi.org/10.1038/s41561-023-01249-5

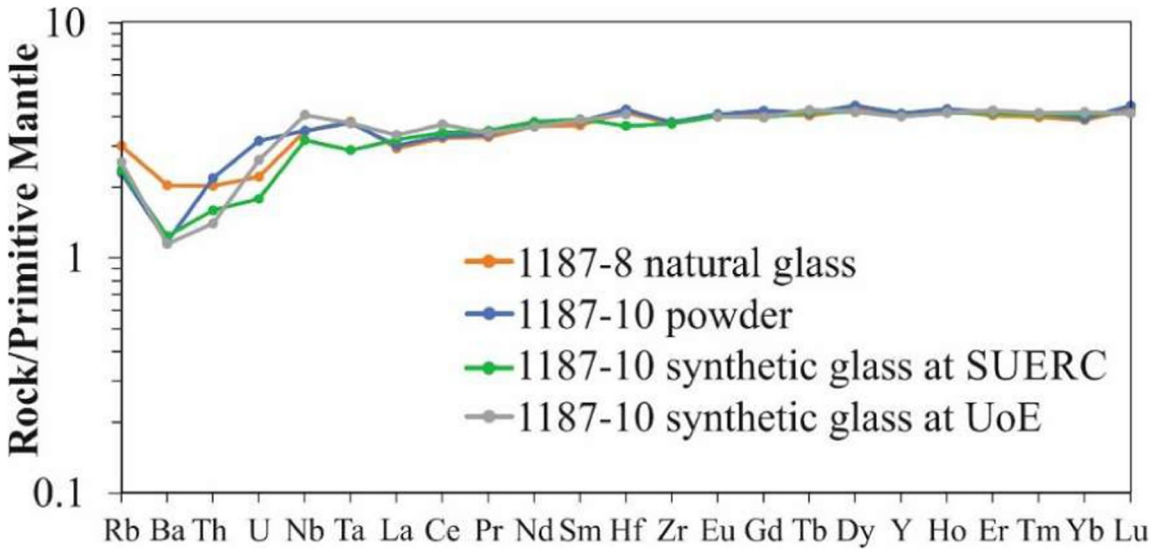

Extended Data Fig. 2 | Trace element compositions. Comparison of starting material trace element compositions.

https://doi.org/10.1038/s41561-023-01249-5

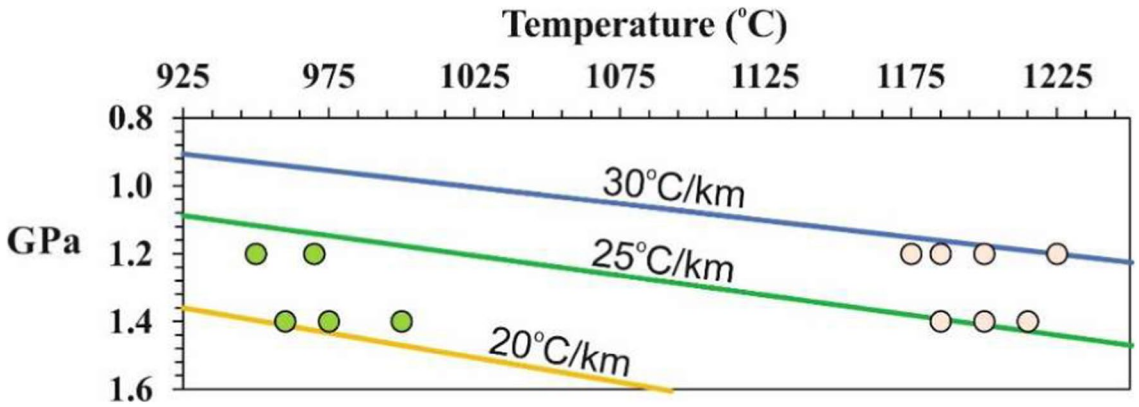

Extended Data Fig. 3 | Geothermal gradients. Diagrammatic cross section through an ~45-km-thick basaltic crust showing 30, 25 and 20 °C/km early Earth geothermal gradients and the pressure-temperature (P-T) conditions of our experimental runs.

https://doi.org/10.1038/s41561-023-01249-5

Extended Data Table 1 | Comparison of major element starting material compositions (wt.%)

	SiO_2	TiO_2	Al_2O_3	FeO	MnO	MgO	CaO	Na_2O	K_2O	P_2O_5
1187-8 natural glass	49.80	0.75	15.04	9.88	0.17	10.01	12.54	1.66	0.09	0.06
1187-10 rock powder	49.56	0.73	15.02	9.85	0.17	10.17	12.67	1.70	0.07	0.06
1187-10 synthetic glass	49.89	0.73	14.53	9.85	0.16	10.20	12.77	1.73	0.10	0.06